JOC The Journal of Organic Chemistry

Article

pubs.acs.org/joc

Rh(I)-Catalyzed Transformation of Propargyl Vinyl Ethers into (*E*,*Z*)-Dienals: Stereoelectronic Role of *trans* Effect in a Metal-Mediated Pericyclic Process and a Shift from Homogeneous to Heterogeneous Catalysis During a One-Pot Reaction

Dinesh V. Vidhani,* Marie E. Krafft, and Igor V. Alabugin*

Department of Chemistry and Biochemistry, Florida State University, Tallahassee, Florida 32306, United States

Supporting Information

ABSTRACT: The combination of experiments and computations reveals unusual features of stereoselective Rh(I)-catalyzed transformation of propargyl vinyl ethers into (*E*,*Z*)-dienals. The first step, the conversion of propargyl vinyl ethers into allene aldehydes, proceeds under homogeneous conditions via a "cyclization-mediated" mechanism initiated by Rh(I) coordination at the alkyne. This path agrees well with the small experimental effects of substituents on the carbinol carbon. The key feature revealed by the computational study is the stereoelectronic effect of the ligand arrangement at the catalytic center. The rearrangement barriers significantly decrease due to the greater transfer of electron density from the catalytic metal center to the CO ligand oriented *trans* to the alkyne. This effect increases electrophilicity of the metal and lowers the calculated barriers by 9.0 kcal/mol. Subsequent evolution of the catalyst leads to the *in situ* formation of Rh(I) nanoclusters that catalyze stereoselective tautomerization. The intermediacy of heterogeneous catalysis by nanoclusters was confirmed by mercury poisoning, temperature-dependent sigmoidal kinetic curves, and dynamic light scattering. The combination of experiments and computations suggests that the initially formed allene-aldehyde product assists in the transformation of a homogeneous catalyst (or "a cocktail of catalysts") into nanoclusters, which in turn catalyze and control the stereochemistry of subsequent transformations.

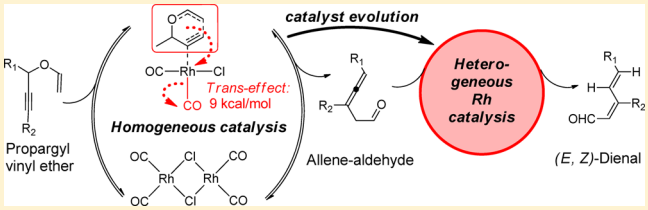

INTRODUCTION

The metal-catalyzed Claisen rearrangement offers new mechanistic paths to this classic reaction and significantly expands its synthetic utility.[1] When metals coordinate with π-bases, such as alkenes or alkynes, the first step of the rearrangement can be described as a *6-endo-dig* cyclization that leads to a cyclic six-membered intermediate (Figure 1). Thus, this mode of rearrangement was termed "cyclization-mediated pathway".[2] On the other hand, Lewis acids such as Cu^{2+}, Al^{3+}, and H^+ initiate the so-called "cation-accelerated oxonia Claisen" rearrangement by coordinating with oxygen (Figure 1).[3]

Recently, we reported a mechanistic study of Au(I)-catalyzed propargyl Claisen and allenyl vinyl ether rearrangement, where Au(I), commonly considered as an alkynophilic Lewis acid, coordinates with the oxygen and directs the Claisen rearrangement through an oxonia path.[4] The barrier for the alternative cyclization-mediated pathway is 1.5 kcal/mol higher. Two important features of the calculated Au-catalyzed cyclization-mediated pathway are (1) lack of substituent effects and (2) selective stabilization of the TS for the Grob fragmentation of the six-membered intermediate by Au(I) catalysts.

The latter effect lowers the barrier to the extent that this intermediate corresponds to a shallow inflection on the potential energy surface, so the overall process blends the characteristics of a stepwise and a concerted process. The nature of this unusual potential energy surface depends strongly on substrate-catalyst coordination and solvent, as illustrated by the successful trapping of the six-membered intermediate by nucleophilic attack of water in dioxane reported by the Toste group.[5]

We were intrigued by the possibility of using deprotonation as a conceptually different approach for trapping the six-membered intermediate. This approach would provide access to conjugated (*E*,*Z*)-dienals via tandem rearrangement of the propargyl vinyl ethers. Such transformation would be synthetically valuable because practical approaches to the thermodynamically less stable (*Z*)-alkenes remain limited in comparison to the variety of methods available for synthesizing the lower energy (*E*)-isomer (Figure 2).[6] Methods for the direct incorporation of the unsaturated α,β -carbonyl compounds, with the Z-stereochemistry at the double bond, remain especially limited.[7]

Guided by this concept, we developed the transformation of propargyl vinyl ethers into (*E*,*Z*)-dienals using a Rh(I)-catalyzed propargyl Claisen rearrangement and prototropic isomerization sequence.[8] This method provides α,β-unsaturated

Received: November 18, 2013
Published: December 4, 2013

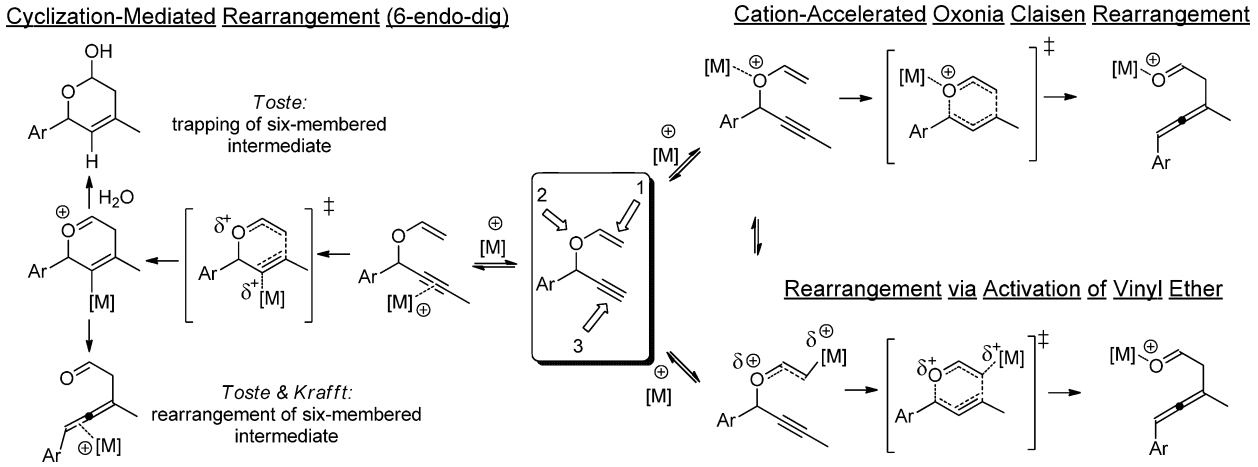

Figure 1. Three mechanistic alternatives for the metal-catalyzed propargyl Claisen rearrangement. Cyclization-mediated pathway dipicted on left shows two possibilities emerging from the six-membered cyclic intermediate.

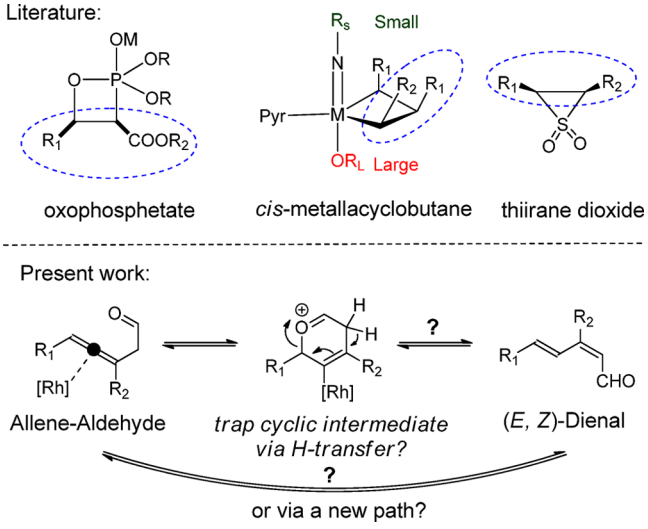

Figure 2. Selected cyclic intermediates in synthesis of (*Z*)-alkenes.

aldehydes from an aldehyde and an alkyne in three steps with excellent stereoselectivity (Figure 3). Catalyst screening showed that propargyl Claisen rearrangement was efficiently catalyzed by several metals, but the stereoselective prototropic rearrangement consistent with a six-membered intermediate was possible only with $[Rh(CO)_2Cl]_2$. Although AuCl also promotes the formation of the dienals, unlike Rh(I) it gives (*E*,*E*)-dienals. The presence of donor ligands at the gold (LAu(I)) does not compromise its ability to catalyze the propargyl Claisen rearrangement but stops the prototropic isomerization step.[9] Optimization studies further revealed that the tandem process was especially efficient in weakly coordinating solvents such as benzene and toluene.

The tandem rearrangement efficiently works for a range of substrates with aromatic, tertiary, and alkenyl substituents at the carbinol carbon (Figure 3). Primary and secondary substituents tend to undergo a further rearrangement to give a mixture of products.

RESULTS AND DISCUSSION

While developing the methodology, we observed that the (*E*,*Z*)-dienal starts to form only after the complete conversion of propargyl vinyl ether into the allene-aldehyde. Thus, we were presented with the opportunity to investigate the kinetics of the two steps of this cascade reaction separately. Initially, we expected that this study would help us to determine whether the transformation of the allene-aldehyde into the (*E*,*Z*)-dienal involves a six-membered organo-Rh(I) intermediate (Figure 2), but our attempts in trapping the proposed six-membered intermediate with a nucleophile or detecting it spectroscopically were not successful, prompting us to investigate this cascade in more detail via a combination of experiments and computations. In particular, we wanted to test whether the allene-diene transformation involves an allene-enol formation, as suggested by Okamura for related reactions,[7] or whether a new alternative exists.

Nonintegral Order in Catalyst. As a first step of our kinetic study, we determined the reaction order with respect to the catalyst by following the rearrangement of phenyl-substituted substrate at different concentrations of the catalyst. A nonlinear fit of the data $f(x) = a(x)^n$ revealed a half order of the Rh(I)-dimer (Figure 4). Such fractional order kinetics has been reported for reactions in which either one of the reactants or the precatalyst dissociate prior to the rate-limiting step.[10] In this system, this observation confirms the dissociation of the dimeric precatalyst into a catalytically active monomeric form (see Supporting Information for the derived rate law).

These experimental results support the model suggested by our preliminary computational study.[8] It was suggested previously that the square planar *d*8 16e$^-$ $[Rh(CO)_2Cl]_2$ precatalyst dissociates into the 14e$^-$ monomeric species prior to catalysis.[11] However, thermodynamic data in Figure 5 illustrate that such dissociation should be assisted by coordination with another ligand, in this case the vinyl ether group of the substrate. This coordination produces new monomeric Rh(I) species responsible for the catalysis of the propargyl Claisen step.

An important consequence of this model is that the fragmentation of the dimer occurs only through an associative mechanism that leads to the formation of the square planar monomer complex with the substrate. The key stereoelectronic feature of this complex is that it is not symmetrical and can have two orientations of the CO ligand relative to the substrate (Figure 6). As we will show in one of the subsequent sections, such differences, which can be considered as a manifestation of

dx.doi.org/10.1021/jo402505f | J. Org. Chem. 2014, 79, 352−364

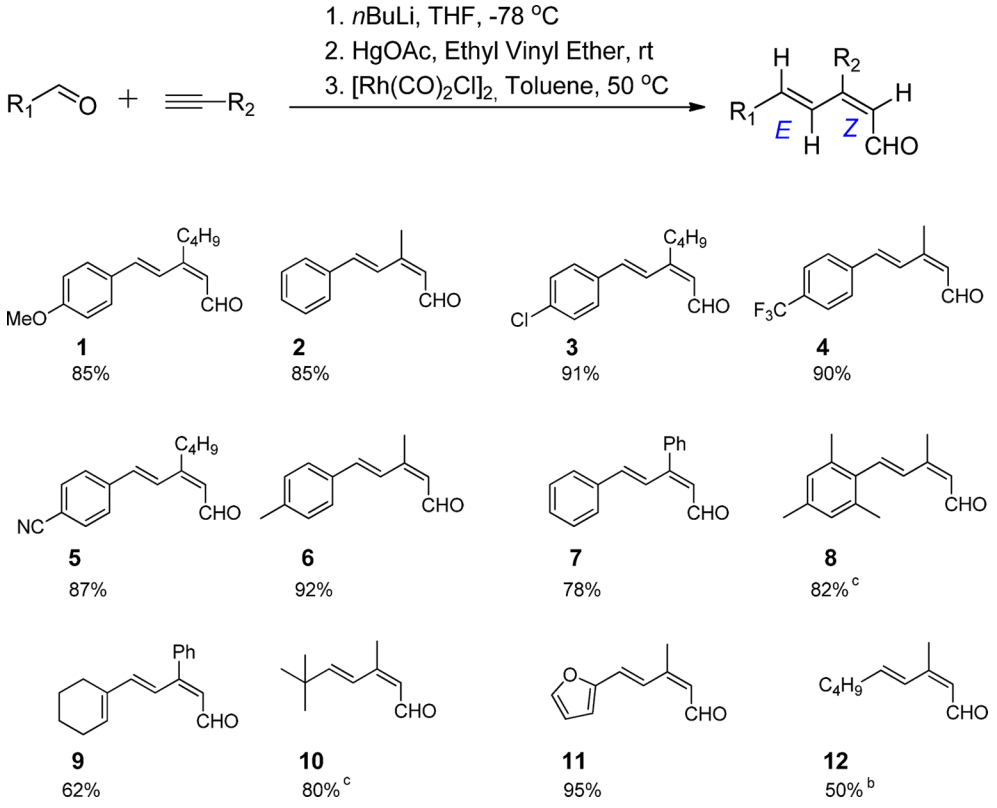

Figure 3. Products and isolated yields of Rh(I)-catalyzed rearrangements obtained from their respective propargyl vinyl ethers. Isomeric ratios were determined using NMR. In all cases the (*E*,*Z*):(*E*,*E*) ratio was found to be >95:5. Reaction conditions: 0.1 M solution of 0.1 mmol propargyl vinyl ether in toluene in the presence of 10% $[Rh(CO)_2Cl]_2$ at 50 °C. Notes: (b) Undergoes further rearrangement to give a mixture of products. (c) Requires 70 °C.

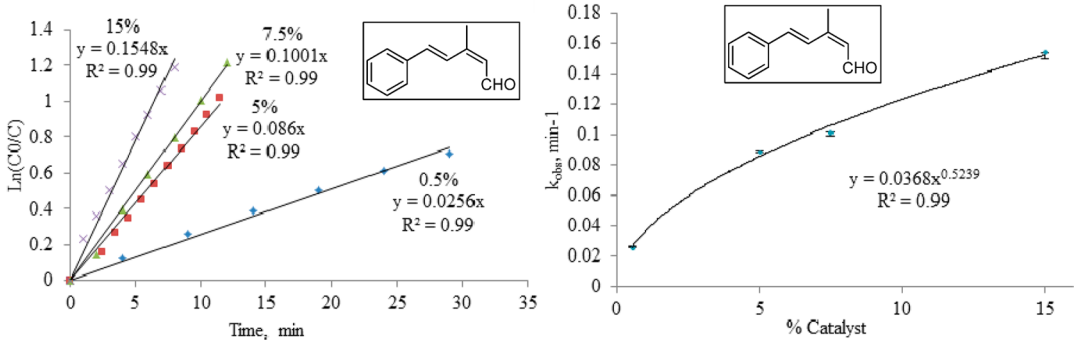

Figure 4. Rate constants determined at four different catalyst concentrations at 330 K for the phenyl-substituted substrate. A nonlinear fit of the data to the equation $f(x) = a(x)^n$ to obtain the order in catalyst concentration.

the *trans*-effect,[12] play a key role in the differences observed transition state.

Substituent Effects. After establishing the order in catalyst, we proceeded in probing the sequence of bond-forming and bond-breaking events in the Claisen part of the catalytic cycle. In the cyclization-mediated pathway, the C4−O3 and C4−C5 bonds should be the least affected (Figure 5). On the other hand, the oxonia Claisen rearrangement is expected to be an asynchronous process, traversing through a dissociative type TS, in which the substituents on the carbinol carbon would significantly influence the C4−O3 bond in the transition state.

Considering the expected differences between the two pathways, we carried out the kinetic study of substrates corresponding to the products **1**−**5** (Figure 3) with the carbinol carbon substituted by electronically different aromatic rings. A clean first-order conversion of all five propargyl vinyl ethers into their respective allene-aldehydes occurs at the chosen range of experimental temperatures. Conveniently, appearance of the final dienal product was not observed at the times when the propargyl vinyl ether was still present. The activation energies, enthalpies, and entropies were obtained using Arrhenius and Eyring equations (see Figure 7 and Supporting Information for the further details).

All five propargyl vinyl ethers show Arrhenius barriers in the range of 14−15 kcal/mol for the transformation into their respective allene-aldehyde (Table 1, see Supporting Information for the kinetic plots). The limited impact of substituents on the carbinol carbon is consistent with a cyclization-mediated model (vide infra). Eyring plots showed large negative entropies of activation. At first sight, this observation may

dx.doi.org/10.1021/jo402505f | J. Org. Chem. 2014, 79, 352−364

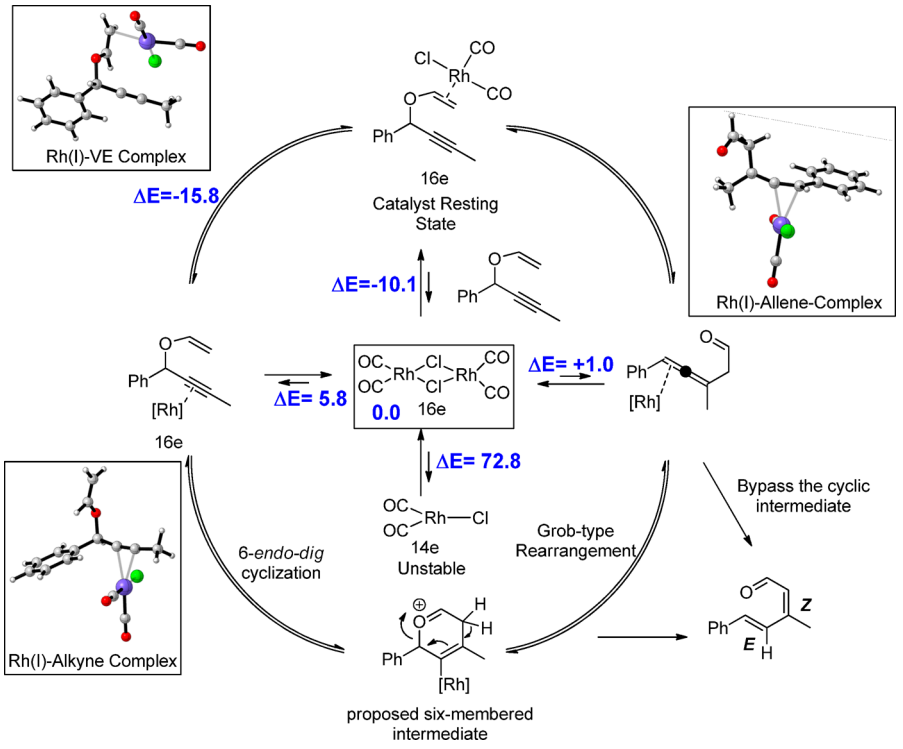

Figure 5. Proposed catalytic cycle. Numbers in blue correspond to the PCM-SCRF-M05-2X/LANL2DZ energies expressed in kcal/mol of the intermediate species relative to the uncomplexed Rh(I)-dimer.

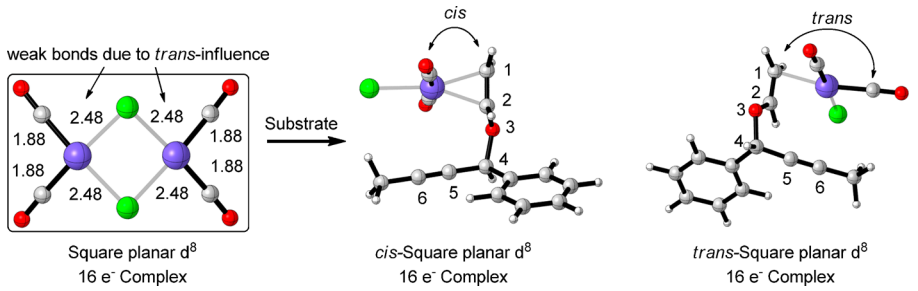

Figure 6. Geometries of the Rh(I)-dimer and the Rh(I)-substrate complexes optimized at the M05-2X/LANL2DZ level.

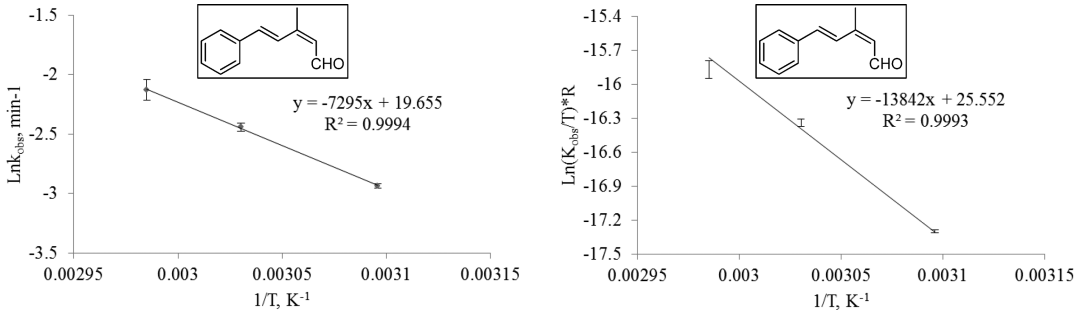

Figure 7. Representative Arrhenius (left) and Eyring (right) plots for the phenyl-substituted substrate **2** obtained by monitoring the Claisen rearrangement at 323, 330, and 335 K.

appear counterintuitive and inconsistent with the fragmentation of Rh(I)-dimer; however, the vinyl ether-assisted fragmentation of Rh(I)-dimer leads to the decrease in the total number of molecules from 3 (Rh(I)-dimer and two substrates) to 2 (two Rh(I)-VE complexes). As a result, this process involves a large negative entropy of activation.

In this selection of substrates, the effects of activation entropy ($\Delta S^{\ddagger}$) and the activation enthalpy ($\Delta H^{\ddagger}$) oppose each other (Table 1; see Figure 45 of Supporting Information). For example, the electron donor (OMe) showed the most favorable entropy of activation, but the effect was compensated by the relatively unfavorable activation enthalpy ($\Delta H^{\ddagger}$ = 14.5 kcal/mol, $\Delta S^{\ddagger}$ = −19.3 cal/K mol). This trend is not followed by the two most electron-deficient substrates **4** and **5.** The deviation was especially large for the nitrile group, where both the enthalpy and entropy of activation were unfavorable, *vide infra*.

dx.doi.org/10.1021/jo402505f | J. Org. Chem. 2014, 79, 352−364

Table 1. Experimental Activation Parameters Obtained Using Arrhenius and Eyring Plots

substrate	E_a kcal/mol	$\Delta H^{\ddagger}$ kcal/mol	$\Delta S^{\ddagger}$ cal/K
PhOMe (**1**)	15.1 ± 0.7	14.5 ± 0.6	−19.4 ± 0.9
Ph (**2**)	14.5 ± 0.7	13.9 ± 0.6	−21.6 ± 0.9
PhCl (**3**)	14.2 ± 0.1	13.5 ± 0.1	−22.7 ± 0.2
p-CF_3-Ph (**4**)	14.6 ± 0.3	13.8 ± 0.3	−23.3 ± 0.4
p-CN-Ph (**5**)	15.1 ± 0.7	14.5 ± 0.6	−22.5 ± 1.0

The experimental entropies suggested fragmentation of precatalyst in all five substrates. In agreement with the proposed cyclization-mediated model, the measured activation barriers show a subtle substituent effect, corroborating the lack of substantial carbinol C−O bond cleavage in the TS. To understand these observations, we undertook a computational study where we compared substituent effects for all three rearrangement pathways.

Computational Methods. The computational analysis of the reaction energy profile for the present rearrangement was performed using DFT formalism as implemented in Gaussian 03. Although the B3LYP is one of the most popular functionals used by the organic chemists, it is also known to often underestimate activation energies[13] and provide unreliable bond energies in transition metal catalysis.[14] On the other hand, the M05-2X functional was shown to perform well for transition metal chemistry, the main group elements, and the calculation of activation barriers.[14] Thus, all geometries were optimized using the M05-2X functional and the LANL2DZ basis sets. Vibrational frequency calculations were performed to confirm the local minima or the transition state corresponding to the given stationary point on the potential energy surface. The transition states were located using the quadratic synchronous transit (QST3) method.[15] For the structurally very similar substrates, the QST-optimized geometries were modified and refined by the restricted transition state search using the Berny algorithm. The solvation energies in toluene were calculated using a self-consisted reaction field on the optimized gas-phase geometries.[16] The Curtin−Hammett barriers were calculated from the most stable Rh(I)-VE complex.

Computational Results. On the basis of the possible coordinating sites on the propargyl vinyl ether, we explored three pathways: (1) cyclization-mediated pathway, (2) Rh(I)-accelerated oxonia Claisen rearrangement, and (3) rearrangement via activation of vinyl ether. In every case, we found that position of the CO ligand (*trans* or *cis*) relative to the substrate had a large role in the reaction.

1. Cyclization-Mediated Pathway. The geometries of reactant-like transition states show that the carbinol C4−O3 and C4−C5 bonds are mostly unaffected during this process. As shown in Figure 8, the C4−O3 (*cis*: 1.47 Å→1.48 Å, *trans*: 1.47 Å→1.48 Å) and C4−C5 bonds are mostly intact in the transition state. Interestingly, C4−C5 bond, which changes from a single bond to a double bond in the final product, shows an initial bond elongation instead of shortening (∼1.48 Å → 1.51 Å for both isomers). The stereoelectronic effect of the *trans*-CO ligand is reflected in the longer incipient C1−C6 distance (*cis*: 2.16 Å vs *trans*: 2.22 Å).

Interestingly, this pathway combines the characteristics of a stepwise and a concerted process. Although only a single TS was located as expected for a concerted reaction, the evolution of aromaticity[17] along the Internal Reaction Coordinate (IRC) (Figure 9) revealed that the maximum aromaticity (NICS(0) = −11.5 ppm) and the most symmetrical geometry were attained at a geometry ∼4.2 kcal/mol downhill from the transition state (NICS(0) = −9.8 ppm). However, even at the maximum of aromaticity, the RMS gradient revealed neither the additional minimum corresponding to the six-membered intermediate nor an inflection indicative[4] of a hidden second transition state (see Supporting Information). These features suggest the interaction

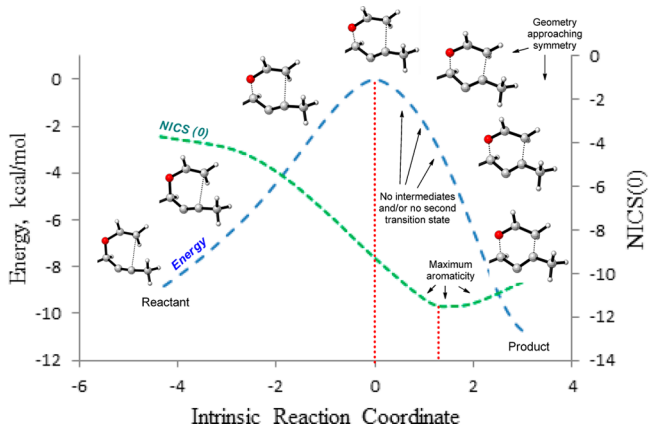

Figure 9. IRC calculations performed at the M05-2X/LANL2DZ level for the Ph-substituted substrate **2** coordinated to Rh(I). The dashed blue line describes changes in energy. The dashed green line corresponds to evolution of aromaticity along the IRC.

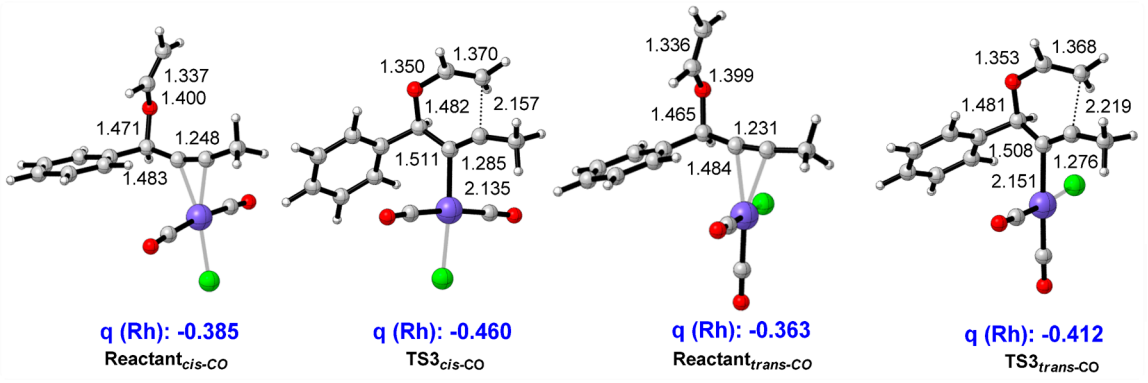

Figure 8. M05-2X/LANL2DZ optimized geometries displaying important bond parameters for the two orientations of CO in the reactant and the TS of the cyclization-mediated pathway. The values in blue color correspond to the NBO charges on rhodium.

dx.doi.org/10.1021/jo402505f | J. Org. Chem. 2014, 79, 352−364

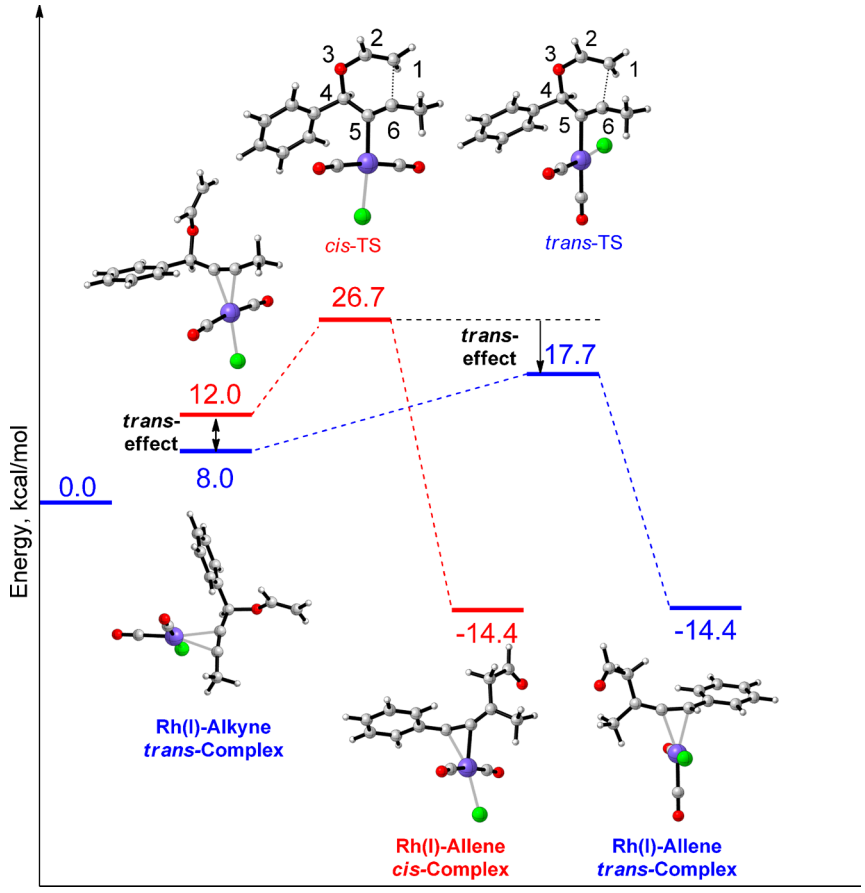

Figure 10. Energy profile of cyclization-mediated pathway. Red and blue color depicts the *cis* and the *trans* orientations of CO, respectively, in the case of phenyl-substituted substrate. Energies were calculated relative to the most stable Rh(I)-VE complex at the M05-2X/LANL2DZ level.

with the catalyst eliminates the Grob fragmentation TS from the reaction hypersurface.

Role of trans-Effect. Large differences for the calculated rearrangement energy surfaces were observed for the two different positions of ligands at the Rh center. These differences correspond to a manifestation of *trans*-effect. The *trans*-effect is defined as the ability of certain ligands to labilize *trans* groups during ligand substitution reactions in square planar complexes.[18] From a conceptual viewpoint, the *trans*-effect can be broadly classified as static and kinetic *trans*-effects.[19] Static *trans*-effect, also known as *trans*-influence or structural *trans*-effect (STE),[20] is a ground state phenomenon where the bonds *trans* to strong σ-donors are significantly elongated. The kinetic *trans*-effect, on the other hand, deals with the stabilization of the trigonal bipyramidal transition state by the strong π-acceptors when such ligands occupy equatorial positions.[21]

In the present study, both the reactant complex and the transition states for the "cyclization-mediated" pathway were significantly stabilized by *trans*-effects of the π-acceptor CO ligand, but as shown in the Figure 10, the transition state is stabilized to a far greater extent (9.0 kcal/mol) than the reactant complex (4.0 kcal/mol).[22] Although barrier heights calculated from the *trans* and *cis* Rh(I)-alkyne complexes were only 9.7 and 14.6 kcal/mol, respectively, the Curtin−Hammett barrier, calculated from the most stable Rh(I)-vinyl ether complex, increases the barrier (17.7 kcal/mol for the *trans*-CO geometry, Figure 10).

The direct involvement of the *trans* carbonyl ligand in the reaction process is further confirmed by parallel trends in the calculated carbonyl IR stretching frequencies and the charge on the metal. Combined, these changes are often used to determine the extent of back-donation from the metal to the π^*-orbital of the CO ligand. In particular, the IR stretching frequency of free CO (2143 cm^{-1}) is reduced to 2120−1850 cm^{-1} when it coordinates to the metal, which has the ability to back-donate electrons into the CO π^*-orbital.[23] For the ground state Rh(I)-alkyne complex, the CO *trans* to the alkyne showed a red shift in the IR CO stretching frequency compared to its *cis* isomer (*cis*: 2082 cm^{-1} vs *trans*: 2040 cm^{-1}). A similar effect was observed for the transition states where the CO that is oriented *trans* to the alkyne is much more effective in dispersing the progressively increasing electron density on Rh(I) and hence shows lower IR CO stretching compared to the *cis* orientation (*cis*: 2036 cm^{-1} vs *trans*: 2027 cm^{-1}).

In this catalytic pathway, Rh(I) serves as a relay in the electronic communication between alkyne and CO ligands. The NBO charges shown in Figure 8 suggest that the metal is far more efficient in shunting electron density when the CO is present *trans* to the alkyne (charge on Rh(I) in *trans*: −0.412 vs *cis*: −0.460). Together, the activation barriers, IR CO stretching frequencies, and NBO charges on the Rh paint a cohesive picture of a stereoelectronic interaction of the *trans*-CO with the alkyne ligand through the metal center.

2. Oxonia Claisen Rearrangement. In the second pathway, coordination of Rh(I) to the oxygen atom of the substrate triggers the cation-accelerated oxonia Claisen rearrangement. This rearrangement proceeds *via* a highly asynchronous pathway with a dissociative-type transition state. The

dx.doi.org/10.1021/jo402505f | J. Org. Chem. 2014, 79, 352−364

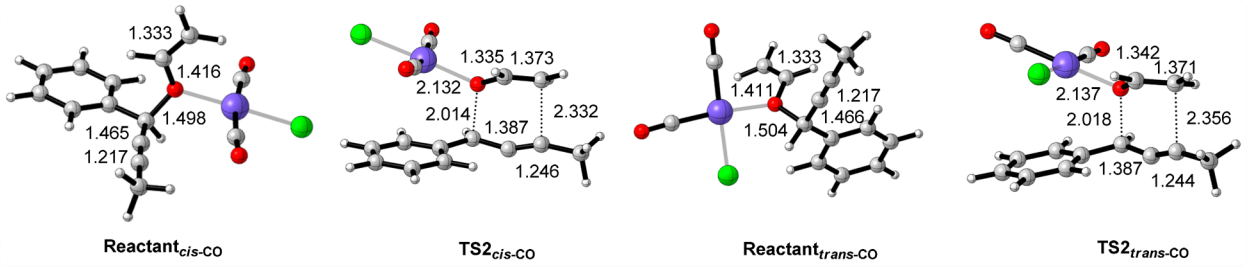

Figure 11. M05-2X/LANL2DZ optimized geometries displaying important bond parameters for the two orientations of CO in the reactant and the TS of cyclization-induced pathway in the case of phenyl-substituted substrate.

fragmentation character is revealed by significant elongation of the carbinol C4−O3 bond (Figure 11, *cis*: 1.50 → 2.01 Å; *trans*: 1.50 → 2.02 Å) in the transition state geometries.

In stark contrast to the selective TS stabilization in the cyclization-mediated pathway, the *trans* orientation of the CO stabilized the ground state oxonia-Claisen reactant more than the transition state (reactant stabilization: 11.1 kcal/mol vs TS stabilization: 10.1 kcal/mol). Due to the unproductive reactant stabilization, the overall Curtin−Hammett barrier (24.4 kcal/mol for the *trans*-CO geometry) remains higher than the barrier for the cyclization-mediated pathway (Figure 12).

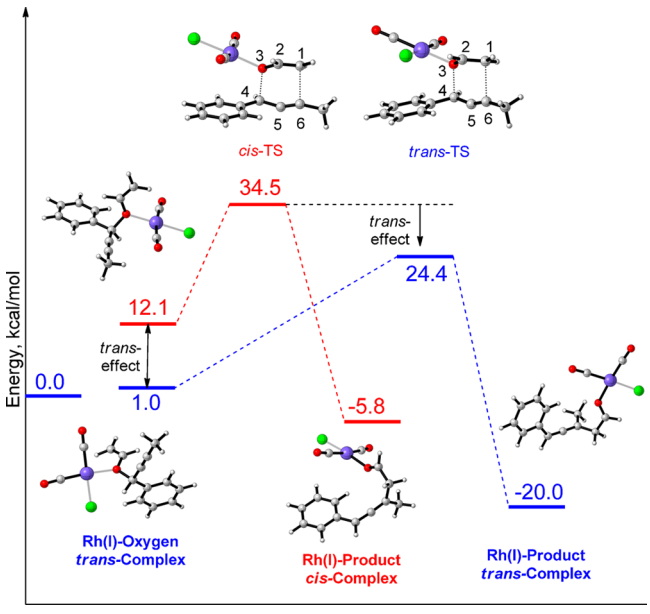

Figure 12. Energy profile of oxonia Claisen pathway in the case of phenyl-substituted substrate. Red and blue color depicts the *cis* and *trans* orientations of CO, respectively. Energies were calculated relative to the most stable Rh(I)-VE complex at the M05-2X/LANL2DZ level.

3. Rearrangement via Activation of the Vinyl Ether. Among the three coordinating sites on the substrate, the π-bond of the vinyl ether forms the most stable complex with the Rh(I) catalyst. Similar to oxonia-Claisen rearrangement, the reaction involves a concerted highly asynchronous pathway with fragmented TS (see Supporting Information for the TS geometries). However, the activation barrier is the highest among the three mechanisms (Figure 13, *trans*-CO: 41.2 kcal/mol). In this path, the *trans*-effect provides only 1 kcal/mol of additional TS stabilization relative to the respective ground state complex.

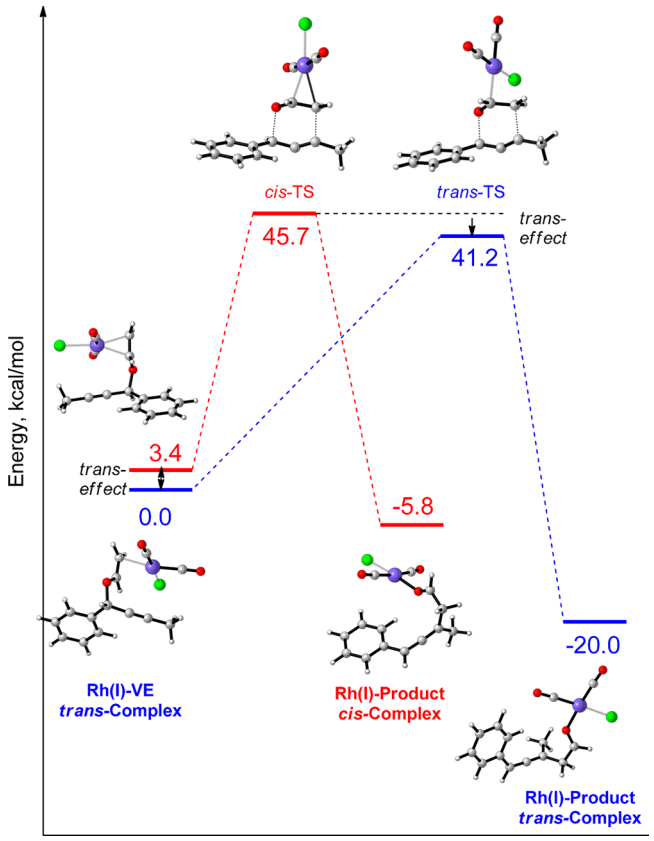

Figure 13. Energy profile of pathway emanating from a Rh(I)-vinyl ether complex in the case of phenyl-substituted substrate. Red and blue color depicts the *cis* and the *trans* orientations of CO, respectively. Energies were calculated at the M05-2X/LANL2DZ level.

In summary, the computational analysis of the three mechanisms suggests that the rearrangement should follow the cyclization-mediated pathway in which one of the CO ligand on the Rh(I) is oriented *trans* to the alkyne.

Correlation of Experimental Barriers with Calculated Barriers. The theory predicts that the carbinol C4−O3 bond is not significantly cleaved in the transition state of the cyclization-mediated pathway. As a result, the substituents at the carbinol carbon are expected to produce relatively small effects. As shown in Table 2, the absolute values of the Curtin−Hammett barriers calculated from the Rh(I)-VE complex (Figure 14) depend on the nature of the most stable complex taken as a reference point in the calculations. Although agreement between the experimental and computational trends is quite good if barriers are calculated relative to complex **A** where the Rh-center displays a cation-π interaction with the

dx.doi.org/10.1021/jo402505f | J. Org. Chem. 2014, 79, 352−364

Table 2. Comparison of Experimental Barriers with the M05-2X and the B3LYP Level Barriers

		M052X/LANL2DZ		B3LYP/LANL2DZ	
substrate	E_a, kcal/mol (exptl)	Curtin–Hammett barrier from the most stable Rh(I) complex	barrier from the alkyne-Rh complex	Curtin–Hammett barrier from the most stable Rh(I) complex	barrier from the alkyne-Rh complex
PhOMe	15.1 ± 0.7	19.4[a] (17.4)	9.6	15.5[a] (15.7)	7.6
Ph	14.5 ± 0.7	18.5[a] (17.7)	9.7	15.5[a] (15.8)	7.7
PhCl	14.2 ± 0.1	17.8[a] (17.2)	9.0	15.1[a] (15.6)	7.1
p-CF3-Ph	14.6 ± 0.3	17.6[a] (16.8)	8.4	14.7[a] (15.1)	6.7
p-CN-Ph	15.1 ± 0.7	19.4[b] (16.9)	8.5	22.2[b] (14.6)	6.8

[a]Values corresponding to square pyramidal Rh(I)-VE complex analogous to structure **B** (Figure 14). Values in parentheses correspond to the square pyramidal Rh(I)-VE complex with alkyne structure **A** (Figure 14). [b]Value correspond to Rh(I)-nitrile complex.

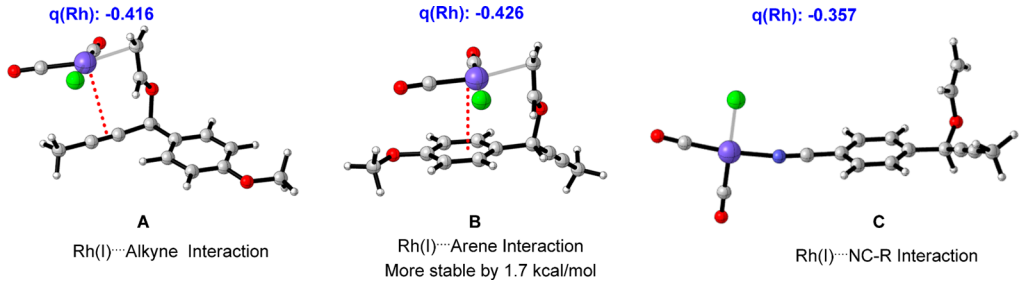

Figure 14. M05-2X optimized geometries of two conformations of the Rh(I)-VE complex. Structure **A** depicts a secondary interaction between Rh(I) and alkyne, and structure **B** depicts an interaction between Rh(I) and arene. Structure **C** shows an interaction between Rh(I) and the nitrogen lone pair of the nitrile substituent. Values in blue color correspond to the NBO charges on Rh(I).

alkyne, the more stable complexes **B**, observed for arenes of good and moderate donor ability, correspond to the cation-π interaction of the Rh center with the arene (Figure 14).[24] In the case of nitrile, the aromatic π-system is a poor partner in the Rh(I)/π-interaction, but the lone pair of nitrile provides a secondary interaction assisting in the formation of the most stable reference complex (**C**,Figure 14). Once the more stable complexes were included in the computations, an excellent correlation (R^2 = 0.989) was found between experimental and computational trends for the four substrates (Figure 15).

Further, we compared the performance of the M05-2X functional with the widely used B3LYP method. Although several B3LYP activation barriers were very close to the experimental values, the overall trend in the B3LYP values failed to follow the experimental trend (Figure 15). The discrepancy is likely to originate from the inability of B3LYP method to describe accurately the noncovalent interactions between the arene and the Rh(I). Further, single point M06-2X calculations with 6-311G(d, p) and aug-cc-pVTZ basis sets showed similar trends in the activation energy for the selected substrates (see Supporting Information for the total energies).

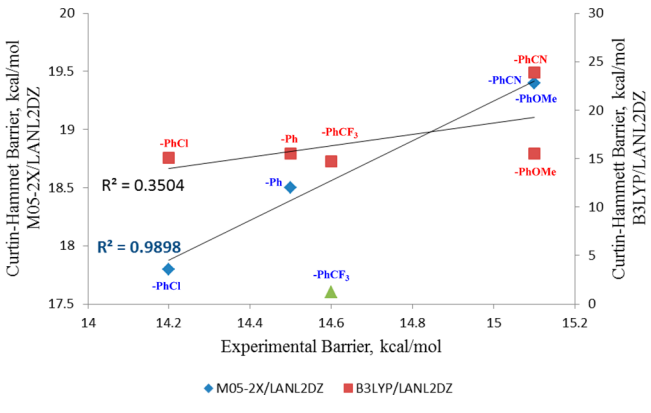

Figure 15. Correlation of experimental and computational Curtin–Hammett barriers. Blue diamonds and red squares correspond to the M05-2X and B3LYP values, respectively. The blue diamond in the top right corner represents two substrates, PhOMe and PhCN (see Table 2). Green triangle represents M05-2X value corresponding to the CF_3-substituted phenyl substrate **4**. Inclusion of this point in the correlation lowers R^2 to 0.75.

Unlike our previous hypothesis, the computational data indicated that deprotonation from the proposed six-membered intermediate in our conditions was unlikely due to the lack of an energy minima corresponding to such an intermediate. Thus, to understand the origin of stereoselectivity, we investigated the second step separately by isolating an allene-aldehyde and subjecting it to the reaction conditions.

Stereoselective Proton Transfer *via* Heterogeneous Catalysis. The combination of olefin isomerization and Claisen rearrangement (the isomerization Claisen rearrangement, or ICR) has been known for quite a long time. The Claisen rearrangement of allyl vinyl ethers that were generated *in situ* from allyl homoallyl ethers were reported to occur in the presence of transition metals such as Ir(I),[25] Ru(II),[26] and Pd(II)[27] catalysts. The tandem stereoselective transition-metal-catalyzed migration of the double bond in allyl homoallyl ethers and ICR was used by several groups to achieve multistep transformation including enantioselective synthesis.[28] However, unlike the literature ICR examples where tautomerization *precedes* the Claisen step, our cascade involves a stereoselective prototropic rearrangement that *follows* the Claisen rearrangement.

A similar transformation of allene-aldehyde to the (*E*,*Z*)-dienal through tandem [1,5] hydride shift, 6π electrocyclic ring closure, and 6π electrocyclic ring opening was reported by Okamura. An essential step needed to enter the Okamura route is enolization of the allene-aldehyde (Figure 16). Our

dx.doi.org/10.1021/jo402505f | J. Org. Chem. 2014, 79, 352–364

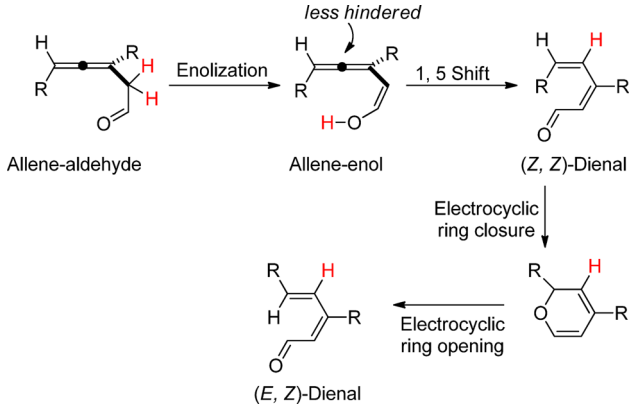

Figure 16. Okamura route to the formation of (*E*,*Z*)-dienal.

experiments found a clean conversion of allene-aldehyde into the (*E*,*Z*)-dienal (Figure 17) with no evidence for the involvement of any intermediates corresponding to the Okamura route (Figure 16).

In addition, the transition state for Rh(I)-catalyzed formation of the (*Z*,*Z*)-dienal was lower in energy (10.2 kcal/mol) than the (*E*,*Z*)-dienal (12.0 kcal/mol) (Figure 18). The formation of single geometric isomer (*E*,*Z*) suggests that the true nature of the active catalyst is different from the proposed monomeric Rh(I) species, which is expected to give a mixture of (*E*,*Z*) and (*Z*,*Z*) geometrical isomers.

Furthermore, the computational analysis of uncatalyzed [1,5] hydrogen shift in allene-enol suggested similar low barriers for the formation of (*E*,*Z*)- (10.7 kcal/mol) and (*Z*,*Z*)-dienals (10.5 kcal/mol) (Figure 18). Thus, the calculations predicted this process does not require catalysis once the allene-enol is formed from the allene-aldehyde and that the reaction should lead to a mixture of the isomers.

This scenario displays an interesting parallel to the work of Ananikov and Beletskaya, who reported the formation of a dynamically evolving mixture of catalytic species in different aggregation states ("cocktail of catalysts") in Pd(II)-catalyzed Heck reactions.[29] The nature of the catalytic species in such situations depends upon the substrate, concentration, temperature, solvents, and additives.

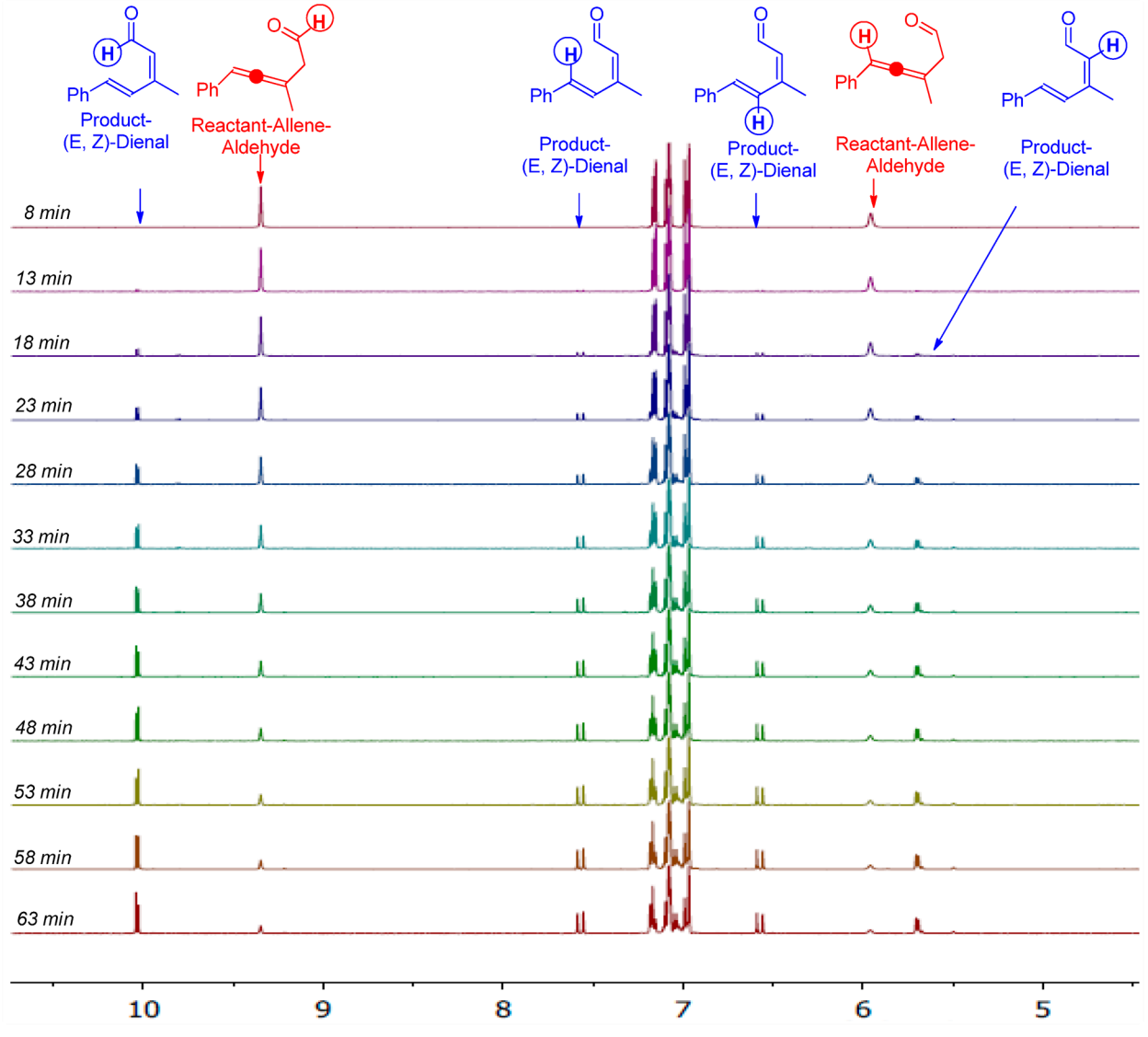

Figure 17. Stacked NMR spectra shows the clean conversion of the allene-aldehyde into the (*E*,*Z*)-dienal.

dx.doi.org/10.1021/jo402505f | *J. Org. Chem.* 2014, 79, 352−364

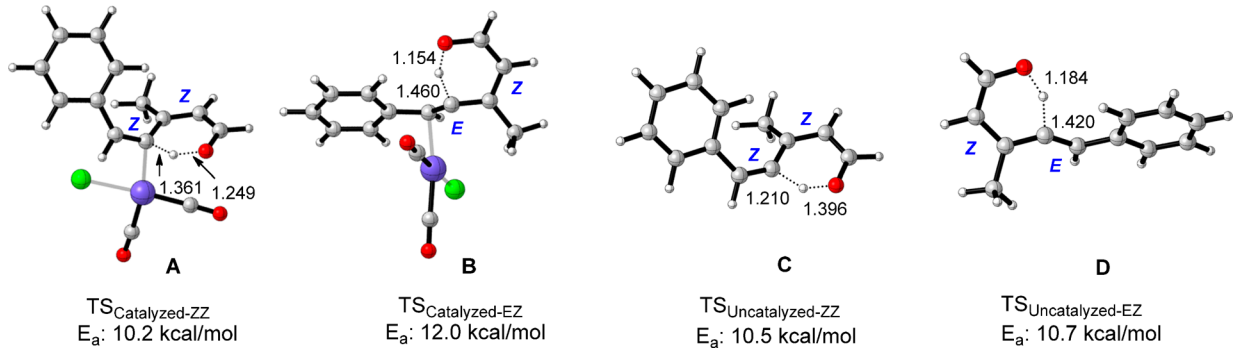

Figure 18. M05-2X optimized transition state geometries of unimolecular [1,5] hydrogen shift. The structures **A** and **B** correspond to the TS geometries of Rh(I)-catalyzed formation of (*Z*,*Z*)- and (*E*,*Z*)-dienals, respectively, whereas structures **C** and **D** correspond to the TS geometries of uncatalyzed formation of (*Z*,*Z*)- and (*E*,*Z*)-dienals, respectively, from the allene-enol.

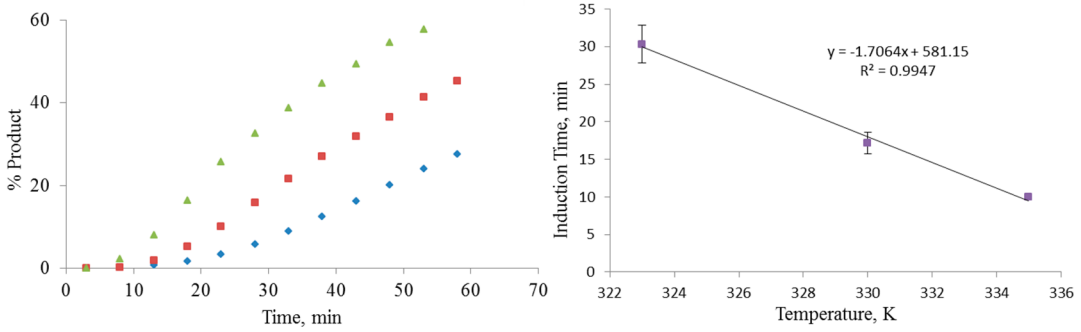

Figure 19. Nonlinear formation of (*E*,*Z*)-dienal **3** from the respective allene-aldehyde. In the plot on the left, the blue diamonds, the red squares, and the green triangles correspond to 323, 330, and 335 K temperature, respectively. Plot on right shows the temperature dependence of the induction time.

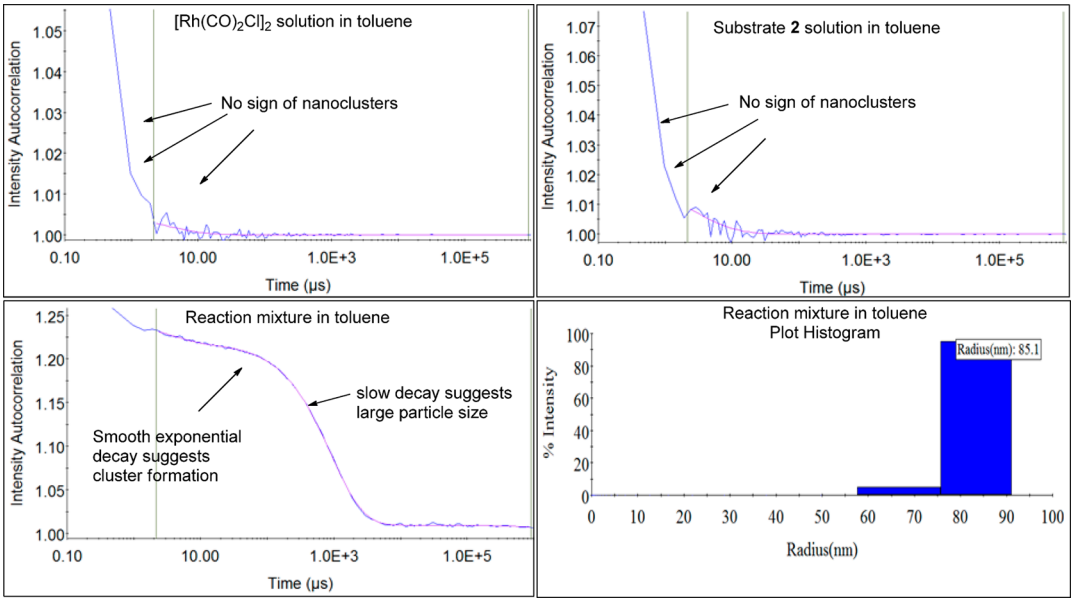

Figure 20. Dynamic light scattering experiment performed on phenyl-substituted substrate **2**. The top two plots correspond to the rates of decay of the autocorrelation function for the catalyst and substrate solutions. The bottom left plot corresponds to the rates of decay of the autocorrelation function for the reaction mixture at 50% conversion. The bottom right plot is a histogram dipicting the particle size (85 nm radius) and 5.2% polydispersity.

We suggest that a similar cocktail of catalysts is formed in our system and that the catalytically active species are Rh nanoparticles. Several experimental observations support this notion. In particular, a sigmoidal correlation between concentrations and reaction times was found instead of exponential first-order decay of allene-aldehyde (Figure 19).[30] The initial induction time was temperature-dependent. Additionally, over a period of 48 h, the solution turned dark brown, and we observed precipitate formation. Several experimental observations such as nonreproducible kinetics[31] at different

dx.doi.org/10.1021/jo402505f | *J. Org. Chem.* 2014, 79, 352−364

metal concentrations, inhibition of the reaction by addition of excess of elemental mercury,[32] and in particular a sigmoidal correlation between concentrations and reaction times instead of exponential first-order decay of allene-aldehyde (Figure 19)[33] lend support to the heterogeneous catalysis hypothesis.[34]

To verify the involvement of nanoparticles in the prototropic rearrangement, we perfromed dynamic light scattering (DLS) experiments on the allene-aldehyde derived from the phenyl-substituted substrate **2**. This technique is used to determine the size distribution of particles in suspension. Typically, in the DLS experiment, the solution containing the nanoclusters is irradiated with monochromatic light from a laser, and the intensity of the light diffracted by the nanocluster is measured. Since the scattered light from nanoclusters undergoes constructive and destructive interference by the surrounding scatterers, a complex intensity fluctuation pattern containing detailed information about the time scale of the movement of the scatterers emerges. To process this information, a mathematical tool called autocorrelation is used to identify a repeating pattern buried under the complex signal:

$$g^2(q;\tau) = \frac{\langle I(t)I(t+\tau)\rangle}{\langle I(t)\rangle^2}$$

where $g^2(q;\tau)$ is the autocorrelation function, q = wave vector, τ = delay time, and I = intensity.

Generally, data is interpreted only when the plot of intensity versus time shows a smooth and continuous decay of intensity for the autocorrelation function. Such plots are classified as "proceed-category". In the present study, the catalyst and the substrate solutions did not show the presence of nanoclusters. Interestingly, the reaction mixture at 50% conversion of allene-aldehyde into respective (*E*,*Z*)-dienal (Figure 20) showed the presence of 170-nm nanoclusters. Moreover, low observed polydispersity (5%) suggested that the solution consisted of uniformly sized particles (Figure 20).

CONCLUSION

In conclusion, experimental and computational analysis of the tandem process suggests a cascade transformation that evolves from homogeneous to heterogeneous catalysis. The Rh(I)-catalyzed propargyl Claisen rearrangement involves homogeneous catalysis, whereas the subsequent prototropic rearrangement shows the telltale signs of heterogeneous catalysis.

Kinetic studies of the Claisen rearrangement showed fractional order in the catalyst. Among three pathways emanating from modes of coordination of Rh(I) with the substrate, the relatively small effects of substituents at the carbinal carbon agreed best with the cyclization-induced pathway. The NICS(0) values suggested that the transition state merged the characteristics of a stepwise and a concerted process (NICS(0) = −12 ppm). Furthermore, the orientation of CO ligands on Rh(I) played a crucial role in determining the barrier heights. Due to the stereoelectronic *trans*-effect, the *trans* orientation of one of the CO ligands relative to the substrate stabilized both the ground state and, to a larger extent, the transition state. This selective stereoelectronic transition state stabilization was estimated to be ∼9 kcal/mol. Trends in substituent effects from the M05-2X calculations agreed well with the experimental order of reactivity, presumably due to the relatively accurate description of the noncovalent interactions by this method. On the other hand, the B3LYP results, despite being numerically close to the experimental barriers, did not correlate well with the trends in experimental substituent effects.

The features indicative of heterogeneous catalysis in the prototropic rearrangement of the allene-aldehyde include the temperature-dependent induction period, sigmoidal shaped curve, nonreproducible kinetics at different catalyst concentrations and the inhibition of reaction in presence of large excess of elemental mercury. Furthermore, DLS experiments confirmed the involvement of 170 nm nanoparticles during the catalysis of second step. We plan to investigate the nature of these clusters, dynamics of their formation as well as the correlation of the nanoparticle structure with their catalytic activity in the future work.

EXPERIMENTAL SECTION

General Procedure for the Synthesis of Substrates. To a 0.1 M solution of 1-phenylbut-2-yn-1-ol (0.146g, 1 mmol) in ethyl vinyl ether (10 mL) was added mercuric acetate (0.6 mmol, 0.190g) in one portion. The reaction mixture was refluxed at 45 °C for 12 h before quenching with a saturated aqueous sodium carbonate solution. The organic phase was extracted using diethyl ether and dried over anhydrous potassium carbonate. The solvent was removed under vacuum, and the crude vinyl ether was purified on alumina gel column using hexane as an eluent. Phenyl-substituted substrate, (1-(vinyloxy)-but-2-yn-1-yl)benzene, was obtained in 60% yield (0.1 g). ^{1}H NMR (500 MHz, CD_2Cl_2) δ: 7.55 (m, 2H), 7.43 (m, 3H), 6.56 (dd, J = 14.1, 6.6 Hz, 1H), 5.54 (q, J = 2.1 Hz, 1H), 4.51 (dd, J = 14.1, 1.8 Hz, 1H), 4.21 (dd, J = 6.6, 1.8 Hz, 1H), 1.97 (d, J = 2.2 Hz, 3H). ^{13}C NMR (125 MHz, CD_2Cl_2) δ: 149.7, 138.5, 128.5, 128.5, 127.2, 89.9, 84.9, 76.2, 71.1, 3.4. Synthesis and spectral data of all functionalized propargyl vinyl ethers corresponding to the compounds **1**−**5** have also been described in our previous work on the stereoselective synthesis of (*E*,*Z*)-dienals.[9]

General Procedure for Kinetic Studies. A stock solution of $[Rh(CO)_2Cl]_2$ (6 mg, 0.015 mmol) was prepared in 0.3 mL of toluene. Another stock solution of (1-(vinyloxy)but-2-yn-1-yl)benzene was prepared in 0.1 M toluene-d_8. The catalyst solution (55 μL,5%, 2.75 μmol) was added to 0.55 mL of the substrate solution at once using a micropipet. The reaction mixture was immediately transferred into the NMR tube and inserted in the 500 MHz NMR machine equilibrated at 323 K. The single pulse acquisitions were obtained automatically after every 120, 300, or 600 s depending upon the temperature. The rate of consumption of vinyl ether and the rate of formation of the product, (*E*,*Z*)-dienal **2**, was monitored using toluene as internal standard. ^{1}H NMR (500 MHz, toluene-d_8) *E*,*Z* δ: 10.05 (d, J = 7.5 Hz, 1H), 7.20−7.03 (m, 5H), 7.53 (d, J = 15.9, 1H), 6.52 (d, J = 16.1 Hz, 1H), 5.71 (dq, J = 7.6, 1.1 Hz, 1H), 1.63 (d, J = 1.1 Hz, 3H). The full information about preparative procedure for the synthesis of products (*E*,*Z*)-dienals **1**−**5** was described in our previous work.[9]

Computational Study. All geometries were optimized at the M05-2X/LANL2DZ and B3LYP/LANL2DZ levels, which frequently performs well for transition metal compounds using the Gaussian 03 program (see Supporting Information for the complete reference). Force field calculation indicated that optimized equilibrium structures were found to be true minima with no imaginary frequency, whereas transition state (TS) geometries had only one imaginary frequency (see Supporting Information). The effect of solvent (toluene) on the reaction barriers was evaluated using single point calculations with the PCM model at the SCRF-M05-2X/LANL2DZ level on the gas-phase geometries. Intrinsic reaction coordinate (IRC) calculations were used to search for intermediates and additional transition states.

ASSOCIATED CONTENT

Supporting Information

Kinetic plots of substrates **1**−**5** at different temperatures. Kinetic plots of substrate **2** at different concentrations.

dx.doi.org/10.1021/jo402505f | J. Org. Chem. 2014, 79, 352−364

Arrhenius and Eyring plots of substarates **1**−**5**. Details of determination of order in catalyst and the rate law. Geometries and energies of all transition states, reactants, and products. Additional experimental details. This material is available free of charge via the Internet at http://pubs.acs.org.

AUTHOR INFORMATION

Corresponding Authors

*E-mail: dineshvidhani16@gmail.com.
*E-mail: alabugin@chem.fsu.edu.

Notes

The authors declare no competing financial interest.

ACKNOWLEDGMENTS

Funding for this project was provided by MDS Research Foundation and NSF Grant CHE-1152491 to I.V.A. We also would like to thank Dr. Virginie Maggiotti (FSU) for helpful discussions, Dr. Steve Freitag (FSU) and Dr. Banghao Chen (FSU) for assistance with variable temperature NMR spectroscopy, Dr. Claudius Mundoma (FSU) for dynamic light scattering experiments, and Dr. Umesh Goli (FSU) for acquiring mass spectra.

REFERENCES

(1) (a) Tejedor, D.; Méndez-Abt, G.; Cotos, L.; García-Tellado, F. *Chem. Soc. Rev.* **2013**, *42*, 458. Aluminium: (b) Bates, D. K.; Janes, M. W. *J. Org. Chem.* **1978**, *43*, 3856. (c) Majumdar, K. C.; Chattopadhyay, B. *Synth. Commun.* **2006**, *36*, 3125. (d) Majumdar, K. C.; Islam, R. *J. Heterocycl. Chem.* **2007**, *44*, 871. (e) Majumdar, K. C.; Islam, R. *Can. J. Chem.* **2006**, *84*, 1632. (f) Majumdar, K. C.; Bhattacharyya, T. *Tetrahedron Lett.* **2001**, *42*, 4231. (g) Majumdar, K. C.; Ghosh, M.; Jana, M.; Saha, D. *Tetrahedron Lett.* **2002**, *43*, 2111. (h) Majumdar, K. C.; Bandyopadhyay, A.; Biswas, A. *Tetrahedron* **2003**, *59*, 5289. Cu(II), Sn(IV), Ti(IV), and La(III): (i) Takanami, T.; Hayashi, M.; Suda, K. *Tetrahedron Lett.* **2005**, *46*, 2893. (j) Trost, B. M.; Schroeder, G. M. *J. Am. Chem. Soc.* **2000**, *122*, 3785. (k) Nakamura, S.; Ishihara, K.; Yamamoto, H. *J. Am. Chem. Soc.* **2000**, *122*, 8131. (l) Nasveschuk, C. G.; Rovis, T. *Org. Lett.* **2005**, *7*, 2173. (m) Nasveschuk, C. G.; Rovis, T. *Angew. Chem., Int. Ed.* **2005**, *44*, 3264. (n) Kaden, S.; Hiersemann, M. *Synlett* **2002**, 1999. (o) Helmboldt, H.; Hiersemann, M. *Tetrahedron* **2003**, *59*, 4031. (p) Abraham, L.; Korner, M.; Hiersemann, M. *Tetrahedron Lett.* **2004**, *45*, 3647. (q) Sharghi, H.; Aghapour, G. *J. Org. Chem.* **2000**, *65*, 2813. (r) Bancel, S.; Cresson, P. *C. R. Acad. Sci. Ser. C* **1970**, *270*, 2161. (s) Nonoshita, K.; Banno, H.; Maruoka, K.; Yamamoto, H. *J. Am. Chem. Soc.* **1990**, *112*, 316. (t) Sugiura, M.; Nakai, T. *Chem. Lett.* **1995**, 697. (u) Akiyama, K.; Mikami, K. *Tetrahedron Lett.* **2004**, *45*, 7217. (v) Itami, K.; Yamazaki, D.; Yoshida, J. *Org. Lett.* **2003**, *5*, 2161. (w) Jamieson, A. G.; Sutherland, A. *Org. Biomol. Chem.* **2006**, *4*, 2932. (x) Swift, M. D.; Sutherland, A. *Org. Biomol. Chem.* **2006**, *4*, 3889. (y) Nakamura, I.; Bajracharya, G. B.; Yamamoto, Y. *Chem. Lett.* **2005**, *34*, 174. (z) Sattelkau, T.; Eilbracht, P. *Tetrahedron Lett.* **1998**, *39*, 1905. (aa) Eilbracht, P.; Gersmeier, A.; Lennard, D.; Huber, T. *Synthesis* **1995**, 330. (ab) Sattelkau, T.; Hollmann, C.; Eilbracht, P. *Synlett* **1996**, 1221. (ac) Sattelkau, T.; Eilbracht, P. *Tetrahedron Lett.* **1998**, *39*, 9647.

(2) (a) Henry, P. M. *Acc. Chem. Res.* **1973**, 16. (b) Henry, P. M. *Adv. Organomet. Chem.* **1975**, *13*, 363. (c) Overman, L. E. *Angew. Chem., Int. Ed. Engl.* **1984**, *23*, 579.

(3) (a) Maruoka, K.; Saito, S.; Yamamoto, H. *J. Am. Chem. Soc.* **1995**, *117*, 1165. (b) Stevenson, J. W. S.; Bryson. *Tetrahedron Lett.* **1982**, *23*, 3143. (c) Takai, K.; Mori, I.; Oshima, K.; Nozaki, H. *Bull. Chem. Soc. Jpn.* **1984**, *57*, 446. (d) Takai, K.; Mori, I.; Oshima, K.; Nozaki, H. *Tetrahedron* **1984**, *40*, 4013. (e) Takai, K.; Mori, I.; Oshima, K.; Nozaki, H. *Tetrahedron Lett.* **1981**, *22*, 3985.

(4) (a) Vidhani, D. V.; Cran, J. W.; Krafft, M. E.; Manoharan, M.; Alabugin, I. V. *J. Org. Chem.* **2013**, *78*, 2059. (b) Vidhani, D. V.; Cran, J. W.; Krafft, M. E.; Alabugin, I. V. *Org. Biomol. Chem.* **2013**, *11*, 1624.

(5) (a) Sherry, B. D.; Maus, L.; Laforteza, B. N.; Toste, D. *J. Am. Chem. Soc.* **2006**, *128*, 8132.

(6) (a) Smith, A. B, III; Beauchamp, T. J.; LaMarche, M. J.; Kaufman, M. D.; Qiu, Y.; Arimoto, H.; Jones, D. R.; Kobayashi, K. *J. Am. Chem. Soc.* **2000**, *122*, 8654. (b) Dong, D.-J.; Li, H.-H.; Tian, S.-K. *J. Am. Chem. Soc.* **2010**, *132*, 5018. (c) Still, W. C. *Tetrahedron Lett.* **1983**, *24*, 4405. (d) Molander, G. A.; Dehmel, F. *J. Am. Chem. Soc.* **2004**, *126*, 10313. (e) Huang, Z.; Negishi, E.-I. *J. Am. Chem. Soc.* **2007**, *129*, 14788. (f) Belardi, J. K.; Micalizio, G. C. *J. Am. Chem. Soc.* **2008**, *130*, 16870. (g) Lindlar, H.; Dubuis, R. *Org. Synth.* **1966**, *46*, 89. (h) Randl, S.; Gessler, S.; Wakamatsu, H.; Blechert, S. *Synlett* **2001**, 430. (i) Kang, B.; Kim, D.-H.; Do, Y.; Chang, S. *Org. Lett.* **2003**, *5*, 3041. (j) Hansen, E. C.; Lee, D. *Org. Lett.* **2004**, *6*, 2035. (k) Kang, B.; Lee, J. M.; Kwak, J.; Lee, Y. S.; Chang, S. *J. Org. Chem.* **2004**, *69*, 7661. (l) Sashuk, V.; Samojlowicz, C.; Szadkowska, A.; Grela, K. *Chem Commun.* **2008**, 2468. (m) Crowe, W. E.; Goldberg, D. R. *J. Am. Chem. Soc.* **1995**, *117*, 5162.

(7) (a) Maynard, D. F.; Okamura, W. H. *J. Org. Chem.* **1995**, *60*, 1763. (b) Duhamel, L.; Guillemont, J.; Poirier, J.-M. *Tetrahedron Lett.* **1991**, *32*, 4495. (c) Cahard, D.; Duhamel, L.; Lecomte, S.; Poirier, J.-M. *Synlett* **1998**, *12*, 1399. (d) Amos, R. A.; Katzenellenbogen, J. A. *J. Org. Chem.* **1978**, *43*, 555.

(8) Vidhani, D. V.; Krafft, M. E.; Alabugin, I. V. *Org. Lett.* **2013**, *15*, 4462.

(9) (a) Sherry, B. D.; Toste, F. D. *J. Am. Chem. Soc.* **2004**, *126*, 15978. (b) Mauleon, P.; Krinsky, J. L.; Toste, F. D. *J. Am. Chem. Soc.* **2009**, *131*, 4513.

(10) (a) Brink, G.-J.; Arends, I. W. C. E.; Papadogianakis, G.; Sheldon, R. A. *Appl. Catal., A* **2000**, *194*−*195*, 435−442. (b) Brink, G.-J.; Arends, I. W. C. E.; Sheldon, R. A. *Adv. Synth. Catal.* **2002**, *344*, 355−369. (c) Steinhoff, B. A.; Guzei, I. A.; Stahl, S. S. *J. Am. Chem. Soc.* **2004**, *126*, 11268. (d) Kholdeeva, O. A.; Kovaleva, L. A.; Maksimovaskya, R. I.; Maksimov, G. M. *J. Mol. Catal. A: Chem.* **2000**, *158*, 223. (e) Alock, N. W.; Brown, J. M.; Conneely, J. A.; Williamson, D. H. *J. Chem. Soc., Chem. Commun.* **1975**, 792. (f) Cook, J.; Hamlin, J. E.; Nutton, A.; Maitlis, P. M. *J. Chem. Soc., Dalton Trans.* **1981**, 2342. (g) Scholten, J. P.; van der Ploeg, H. J. *J. Polym. Sci. Polym. Chem. Ed.* **1973**, *11*, 3205.

(11) (a) Pitcock, W. H., Jr.; Lord, R. L.; Baik, M.-H. *J. Am. Chem. Soc.* **2008**, *130*, 5821. (b) Williams, V. M.; Kong, J. R.; Ko, B. J.; Mantri, Y.; Brodbelt, J. S.; Baik, M. H.; Krische, M. J. *J. Am. Chem. Soc.* **2009**, *131*, 16054.

(12) (a) Connelly, N. G.; Emslie, D. J. H.; Geiger, W. E.; Hayward, O. D.; Linehan, E. B.; Orpen, A. G.; Quayle, M. J.; Rieger, P. H. *J. Chem. Soc., Dalton Trans.* **2001**, 670. (b) Abel, E. W.; Gelling, A.; Orrell, K. G.; Osborne, A. G.; Šik, V. *Chem. Commun.* **1996**, 2329. (c) Haake, P.; Pfeiffer, R. M. *Chem. Commun.* **1969**, 1330. (d) Haake, P.; Pfeiffer, R. M. *J. Am. Chem. Soc.* **1970**, *92*, 4996. (e) Haake, P.; Pfeiffer, R. M. *J. Am. Chem. Soc.* **1970**, *92*, 5243. (f) Braterman, P. S.; Cross, R. J. *Chem. Soc. Rev.* **1973**, *2*, 271.

(13) Zhao, Y.; González-García, N.; Truhlar, D. G. *J. Phys. Chem. A* **2005**, *109*, 2012.

(14) (a) Tsipis, A. C.; Orpen, A. G.; Harvey, J. N. *Dalton Trans.* **2005**, 2849. (b) Zhao, Y.; Truhlar, D. G. *Org. Lett.* **2007**, *9*, 1967. (c) Reiher, M.; Salomon, O.; Hess, B. A. *Theor. Chem. Acc.* **2001**, *107*, 48. (d) Schultz, N.; Zhao, Y.; Truhlar, D. G. *J. Phys. Chem. A* **2005**, *109*, 4388. (e) Schultz, N.; Zhao, Y.; Truhlar, D. G. *J. Phys. Chem. A* **2005**, *109*, 11127. (f) Harvey, J. N. *Annu. Rep. Prog. Chem., Sect. C: Phys. Chem.* **2006**, *102*, 203.

(15) (a) Peng, C.; Schlegel, H. B. *Isr. J. Chem.* **1993**, *33*, 449. (b) Peng, C.; Ayala, P. Y.; Schlegel, H. B *J. Comput. Chem.* **1996**, *17*, 49.

(16) (a) Marten, B.; Kim, K.; Cortis, C.; Friesner, R. A.; Murphy, R. B.; Ringnalda, M. N.; Sitkoff, D.; Honig, B. *J. Phys. Chem.* **1996**, *100*, 11775. (b) Friesner, R. A.; Murphy, R. B.; Beachy, M. D.; Ringnalda,

M. N.; Pollard, W. T.; Dunietz, B. D.; Cao, Y. X. *J. Phys. Chem. A* **1999**, *103*, 1913.
(17) Such analysis has been useful in understanding pericyclic reactions. See ref 2 and Gilmore, K.; Manoharan, M.; Wu, J.; Schleyer, P. v. R.; Alabugin, I. V. *J. Am. Chem. Soc.* **2012**, *134*, 10584.
(18) (a) Chernyaeiv, I. *Ann. Inst. Platine* **1926**, *4*, 261. Drew, H. D. K. *J. Chem. Soc.* **1932**, 2328. (b) Drew, H. D. K.; Pinkard, F. W.; Preston, G. H.; Wardlaw, W. *J. Chem. Soc.* **1932**, 1895. (c) Drew, H. D. K.; Pinkard, F. W.; Preston, G. H.; Wardlaw, W.; Cox, E. G. *J. Chem. Soc.* **1932**, 1004. (d) Jorgensen, S. M. *Z. Anorg. Chem.* **1900**, *24*, 171. Basolo, F.; Pearson, R. G. *Prog. Inorg. Chem.* **1962**, *4*, 381. (e) Pidcock, A.; Richards, R. E.; Venanzi, L. M. *J. Chem. Soc. A* **1966**, 1707. (f) Quagliano, J. V.; Schubert, L. *Chem. Rev.* **1952**, *50*, 201. (g) Appleton, T. G.; Clark, H. C.; Manzer, L. E. *Coord. Chem. Rev.* **1973**, *10*, 335. (h) Hartley, F. R. *Chem. Soc. Rev.* **1973**, *2*, 163. (i) Yatsimirskii, K. B. *Pure Appl. Chem.* **1974**, *38*, 341. (j) Nekrasov, B. V. *J. Gen. Chem. USSR* **1937**, *7*, 1594. (k) Chatt, J.; Duncanson, L. A.; Venanzi, L. M. *J. Chem. Soc.* **1955**, 4456. (l) Orgel, L. E. *J. Inorg. Nucl. Chem.* **1956**, *2*, 137. (m) Basolo, F.; Chatt, J.; Gray, H. B.; Pearson, R. G.; Shaw, B. L. *J. Chem. Soc.* **1961**, 2207. (n) McWeeny, R.; Mason, R.; Towl, A. D. C. *Discuss. Faraday Soc.* **1969**, *47*, 20. (o) Mason, R.; Towl, A. D. C *J. Chem. Soc. A* **1970**, 1601. Bright, D.; Ibers, J. A. *Inorg. Chem.* **1969**, *8*, 709. (p) Shustorovich, E. M.; Porai-Koshits, M. A.; Buslaev, Y. A. *Coord. Chem. Rev.* **1975**, *17*, 1. (q) Burdett, J. K.; Albright, T. A. *Inorg. Chem.* **1979**, *18*, 2112. (r) Lyne, P. D.; Mingos, D. M. P. *J. Organomet. Chem.* **1994**, *478*, 141. (s) Lyne, P. D.; Mingos, D. M. P. *J. Chem. Soc., Dalton Trans.* **1995**, 1635.
(19) Lin, Z.; Hall, M. B. *Inorg. Chem.* **1991**, *30*, 646.
(20) Coe, B. J.; Glenwright, S. J. *Coord. Chem. Rev.* **2000**, *203*, 5.
(21) Square planar complexes undergo ligand substitution reaction through an associative mechanism whereby the metal receives electron density from the incoming ligand. Thus the ability of the strong π-acceptors to disperse the developing negative charge on the metal gives rise to the kinetic *trans*-effect. On the basis of the strength of ligand, the spectrochemical series for the combined static and kinetic *trans*-effect can be summarized as C_2H_4, CO, CN^- > PR_3, H^- > CH_3^- > C_6H_5, NO_2^-, SCN^-, I^- > Br^-, Cl^- > Py, NH_3, OH^-, H_2O
(22) Transition state stabilization is a particularly attractive strategy for accelerating pericyclic reactions. For recent examples, see: (a) Gold, B.; Schevchenko, N.; Bonus, N.; Dudley, G. B.; Alabugin, I. V. *J. Org. Chem.* **2012**, *77*, 75. (b) Gold, B.; Dudley, G. B.; Alabugin, I. V. *J. Am. Chem. Soc.* **2013**, *135*, 1558.
(23) The extent of the red shift depends upon the charge on the metal, the nature of other ligands coordinated to the metal, and the symmetry of the metal complex. Interestingly, the π-backbonding weakens when the two strong π-acceptors are oriented *trans* to each other and strengthens when a π-acceptor is *trans* to the strong σ-donor. However, alkynes, which are both the σ-donor and π-acceptor, compete with the CO for the M → L π-backdonation.
(24) In the present study, the *p*-OMe group did not reveal the stereoelectronically governed dichotomous behavior found in anionic reactions: Peterson, P. W.; Shevchenko, N.; Alabugin, I. V. *Org. Lett.* **2013**, *15*, 2238.
(25) (a) Higashino, T.; Sakaguchi, S.; Ishii, Y. *Org. Lett.* **2000**, *2*, 4193. (b) Notre, J. L.; Brissieux, L.; Semeril, D.; Bruneau, C.; Dixneuf, P. H. *Chem. Commun.* **2002**, 1772. (c) Nelson, S. G.; Bungard, C. J.; Wang, K. *J. Am. Chem. Soc.* **2003**, *125*, 13000. (d) Nelson, S. G.; Wang, K. *J. Am. Chem. Soc.* **2006**, *128*, 4232.
(26) (a) Schmidt, B. *Synlett* **2004**, 1541−1544. Schmidt, B. *Eur. J. Org. Chem.* **2004**, 1865. (b) Louie, J.; Grubbs', R. H. *Organometallics* **2002**, *21*, 2153. (c) Dinger, M. B.; Mol, J. C. *Organometallics* **2003**, *22*, 1089. (d) Yi, C. S.; Lee, D. W. *Organometallics* **1999**, *18*, 5152.
(27) Nevado, C.; Echavarren, A. M. *Tetrahedron* **2004**, *60*, 9735.
(28) (a) Ebel, H.; Knor, S.; Steglish, W. *Tetrahedron* **2002**, *59*, 123. (b) Luzung, M. R.; Toste, F. D. *J. Am. Chem. Soc.* **2003**, *125*, 15760.
(29) (a) Ananikov, V. P.; Beletskaya, I. P. *Organometallics* **2012**, *31*, 1595. (b) Beletskaya, I. P.; Ananikov, V. P. *Chem. Rev.* **2011**, *111*, 1596. (c) Beletskaya, I. P.; Ananikov, V. P. *Eur. J. Org. Chem.* **2007**, 3431. (d) Beletskaya, I. P.; Ananikov, V. P. *Pure Appl. Chem.* **2007**, *79*, 1041. (e) Ananikov, V. P.; Beletskaya, I. P. *Dalton Trans.* **2011**, *40*, 4011.
(30) (a) Widegreen, J. A.; Finke, R. G. *J. Mol. Catal. A: Chem.* **2003**, *198*, 317. (b) Widegreen, J. A.; Bennett, M. A.; Finke, R. G. *J. Am. Chem. Soc.* **2003**, *125*, 10301.
(31) (a) Lin, Y.; Finke, R. G. *Inorg. Chem.* **1994**, *33*, 4891. (b) Laine, R. M. *J. Mol. Catal.* **1982**, *14*, 137.
(32) (a) Crabtree, R. H.; Mellea, M. F.; Mihelcic, J. M.; Quirk, J. M. *J. Am. Chem. Soc.* **1982**, *104*, 107. (b) Anton, D. R.; Crabtree, R. H. *Organometallics* **1983**, *2*, 855. (c) Whitesides, G. M.; Hackett, M.; Brainard, R. L.; Lavalleye. J. P. M.; Sowinski, A. F.; Izumi, A. N.; Moore, S. S.; Brown, D. W. (d) Staudt, E. M. *Organometallics* **1985**, *4*, 181 9. (e) Lewis, L. N.; Lewis, N. *J. Am. Chem. Soc.* **1998**, *108*, 7228. (f) Lewis, L. N.; Uriarte, R. J. *J. Mol. Catal.* **1991**, *66*, 105.
(33) (a) Widegreen, J. A.; Finke, R. G. *J. Mol. Catal. A: Chem.* **2003**, *198*, 317. (b) Widegreen, J. A.; Bennett, M. A.; Finke, R. G. *J. Am. Chem. Soc.* **2003**, *125*, 10301.
(34) (a) Collman, J. P.; Hegedus, L. S.; Norton, J. R.; Finke, R. G. *Principles and Applications of Organotransition Metal Chemistry*; University Science Books: Mill Valley, CA, 1987. (b) Collman, J. P.; Kosydar, K. M.; Bressan, M.; Lamanna, W.; Garrett, T. *J. Am. Chem. Soc.* **1984**, *106*, 2569. (c) Hamlin, J. E.; Hirai, K.; Millan, A.; Maitlis, P. M. *J. Mol. Catal.* **1980**, *7*, 543. (d) Anton, D. R.; Crabtree, R. H. *Organometallics* **1983**, *2*, 855. (e) Crabtree, R. H.; Mellea, M. F.; Mihelcic, J. M.; Quirk, J. M. *J. Am. Chem. Soc.* **1982**, *104*, 107. (f) Crabtree, R. H.; Mihelcic, J. M.; Quirk, J. M. *J. Am. Chem. Soc.* **1979**, *101*, 7738.